Proceedings of the 8th World Congress on Mechanical, Chemical, and Material Engineering (MCM'22)
Prague, Czech Republic – July 31, 2022 - August 02, 2022
Paper No. HTFF 156
DOI: 10.11159/htff22.156

Experimental Investigation on Pressure Drop In Liquid-Liquid Taylor Flow Regimes

Seyyed Saeed Shojaee Zadeh[1,2], Vanessa Egan[1,2], Pat Walsh[1,2]
[1] School of Engineering, University of Limerick, Ireland, V94T9PX
[2]CONNECT, Stokes Laboratories, Bernal Institute, University of Limerick, Ireland, V94T9PX
Saeed.zadeh@ul.ie, Vanessa.egan@ul.ie, Pat.walsh@ul.ie

Abstract **-** This study presents an experimental investigation on pressure drop in liquid-liquid Taylor flow regimes with the objective of extending previous research carried out on this topic. Pressure drop measurements were obtained over a wide range of Capillary ($2.9 \times 10^{-4} \leq Ca \leq 5.1 \times 10^{-2}$) and Reynolds ($0.17 \leq Re \leq 45$) numbers while carrier to dispersed viscosity ratio (μ^*) spanned from 0.059 to 23.2. Five different liquid-liquid flow combinations were examined within capillaries of diameter $0.8mm$. Analysis of existing models from relevant literature reveals that they are limited to specific ranges of Reynolds and Capillary numbers and not sufficiently accurate to predict pressure drop values over a wide range of viscosity ratios. Through comparison with experimental data from this study, the strengths and weaknesses of these models are identified and a more fundamental understanding of predicting pressure drop in Taylor flow regimes is developed.

Keywords**:** experimental, pressure drop, liquid-liquid, Taylor flow, viscosity ratio

1. Introduction

Slug flows in microchannels with high surface-to-volume ratios and internal circulations significantly promote heat transfer from the channel wall[1, 2]. In recent decades, the weakness of traditional thermal management systems has been more evident due to a massive increase in heat flux in electronics components and significant downsizing. Using forced air convection methods enable us to reach almost up to heat flux of 150 $W.cm^{-2}$ [3] while in some cases like laser diode arrays heat flux can skyrocket to 1000 $W.cm^{-2}$ [4]. Applying direct liquid cooling, such as pool boiling, jet impingement and spray cooling[5-7] can provide a high heat transfer coefficient by taking benefit of the latent heat of the liquids. Despite the attractive thermal behaviour of direct liquid cooling systems with or without phase change, these methods are still insufficient and more complex from the use and design point of view which require additional maintenance procedures for hot swapping electronic parts[8].

In all systems that benefit slug flows, a reliable pressure drop prediction is required to estimate the correct power consumption and secure a desired flow rate. In response to this demand, researchers conducted a variety of experimental and numerical research throughout the last few years, resulted in a few correlations mainly focused on liquid-gas flows. In comparison, for liquid-liquid flows only a few studies exist which have focused on modelling pressure drop.

Among the existing models, stagnant-film and moving-film models proposed by Jovanović *et al*.,[9] as well as the skin-friction model by Mac Giolla Eain *et al*.,[10], are the most generally accepted and widely referenced pressure drop models for liquid-liquid Taylor flows. Jovanović *et al.,[9]* developed two correlations based on two different assumptions; (1) by assuming stagnant liquid film and (2) by assuming moving liquid film. Their findings revealed that film velocity has no effect on pressure drop. As a result, both models were found to predict quite similarly, and the stagnant film model was determined to be accurate enough for pressure drop estimation. They performed their experiments by means of two capillaries with inlet diameters of $248\mu m$ and $498\ \mu m$ and three different liquids of water, toluene and ethylene glycol while, Reynolds and Capillary number ranges were of $1.9 - 84.4$ and $6.9 \times 10^{-4} - 1.9 \times 10^{-2}$ respectively. Mac Giolla Eain *et al.,[10]* conducted an experimental study over a range of variables resulting in a correlation to determine the skin friction coefficient for liquid-liquid slug flows by focusing on the interfacial contribution to overall pressure drop. In their experiments, carrier to dispersed viscosity ratio ranged between $\sim 1.3\ to\ \sim 21$. The proposed correlation from this study was found to be in good agreement with experimental results, with the majority of data points falling within 15% error band width of the model.

From a review of relevant published studies, the majority of work has focused on flows with a carrier to dispersed phase viscosity ratios greater than unity which is similar to liquid-gas flows. However, in liquid-liquid flows, a liquid with a comparably lower viscosity can segment the dispersed phase. In liquid-gas slug flows the viscosity of the carrier phase is always much greater than the dispersed phase ($\mu_C/\mu_D \gg 1$) which results in negligible gaseous frictional losses. While in liquid-liquid slug flows, an increased contribution of the dispersed phase to pressure drop has made the prediction more complicated and depending on the viscosity ratio of the involved fluids, the interfacial tension can significantly influence the overall pressure drop[11].

To address this concern, the current research presents a set of measurements spanning a wide range of dimensionless parameters including, Reynolds numbers from 0.17 to 45, Capillary numbers from 2.9×10^{-4} to 5.1×10^{-2}, Weber numbers from 7.1×10^{-4} to 1.6, carrier to dispersed viscosity ratios from 0.059 to 23.2, and slug length to diameter ratios from 3.3 to 15.3. To achieve this, five different liquid-liquid combinations were tested in capillaries with nominal inner diameters of 0.8mm. A novel apparatus was developed to accurately determine the length and velocity of each carrier/dispersed phase unit in the system. A comprehensive comparison is made between experimental results and the existing pressure drop models from literature[9, 10] and limitations with the models are identified.

2. Theory

In liquid-liquid slug flow regimes, the overall pressure drop (ΔP_T) is defined as the sum of frictional pressure drop in the carrier (ΔP_C) and dispersed (ΔP_D) phase and interfacial pressure drop (ΔP_{Int}) due to the interface between the two phases.

$$\Delta P_T = \Delta P_C + \Delta P_D + \Delta P_{Int} \tag{1}$$

The pressure drop across the carrier phase (ΔP_C) can be simply characterized by the Hagen-Poiseuille equation ($\Delta P = 32\mu UL/D^2$) by knowing the flow viscosity (μ), flow velocity (U), capillary length (L), and diameter (D) assuming fully-developed laminar flow with a parabolic velocity profile across the channel. To predict the pressure along the dispersed phase, Jovanović *et al.*[9] proposed two different models known as stagnant-film and moving-film models. In the moving-film model as shown in Eq. 2, total pressure drop can be significantly affected by film thickness.

$$\frac{\Delta P_T}{L} = \frac{8\mu_C U(1-\varepsilon)}{R^2} + \frac{4\mu_D U_D \varepsilon}{\frac{(R^2-(R-h)^2)}{\mu_C} + \frac{(0.5(R-h)^2)}{\mu_D}} + \frac{1}{L_u} 7.16(3Ca_C)^{2/3} \frac{\gamma}{D} \tag{2}$$

Where μ_C, ε, R, μ_D, U_D, h, L_u, γ and Ca_C refer to carrier viscosity, droplet length fraction ($\varepsilon = L_D/L_u$), capillary radius, droplet viscosity, droplet velocity, film thickness, slug unit length ($L_u = L_D + L_C$), interfacial surface tension between respective phases and the Capillary number based on the carrier phase properties respectively. In equation 2, the contribution of the interfacial pressure drop (last term) is calculated using Bretherton's equation[12].

Equation 3 presents the stagnant-film model which only the middle term, describing contribution of the dispersed phase, differs from the previous model in Eq. 2.

$$\frac{\Delta P_T}{L} = \frac{8\mu_c U(1-\varepsilon)}{R^2} + \frac{8\mu_D U_D \varepsilon}{(R-h)^2} + \frac{1}{L_u} 7.16(3Ca_C)^{2/3} \frac{\gamma}{D} \tag{3}$$

Mac Giolla Eain *et al*.,[10] established a new model focused on the contribution of interfacial pressure drop to overall pressure drop in liquid-liquid Taylor flows using a semi-empirical method and a different technique than the differential Laplace pressure. Assuming the exact approximation of single phase theory in obtaining the pressure drop along both phases, the interfacial pressure drop is calculated by subtracting the oil and water pressure drops form the total experimentally measured pressure drop. The interfacial pressure drop is stated in the form of a dimensionless skin-friction factor (C_f) presented in the following equation.

$$C_f = 14.486[({L_D^*}^{0.65}) \times (Ca_C^{-0.616}) \times (Re_C^{-1.05})] \tag{4}$$

The skin-friction coefficient is determined as a function of dimensionless droplet length ($L_D^* = {L_D}/{D}$), Capillary and Reynolds number in this equation. Where subscripts C and D refer to the carrier and dispersed phases respectively. This scaling group correlates the interfacial pressure drop and was achieved by a regression analysis of the data.

3. Experimentation

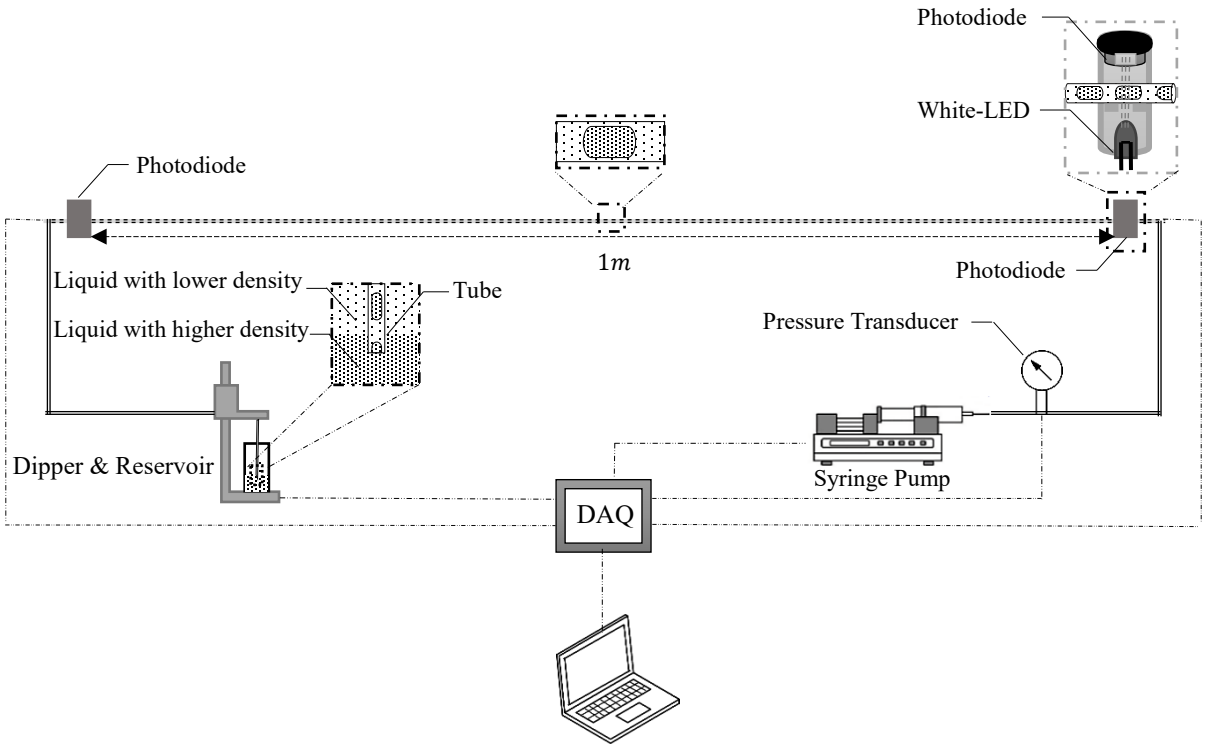

Fig. 1: Experimental configuration used for pressure drop, slug length and velocity measurements

The experimental configuration used to measure pressure drop, slug length and velocity is shown in Fig. 1. Droplet trains were generated in a 0.8mm ID, 4.5m length FEP Teflon tube (horizontally oriented) using a custom designed traverse stage and reservoir. In order to generate consistent slug trains, the tube was firstly primed with the carrier liquid. Following this, both liquids were drawn into the tube by running a Harvard Pico Plus Elite syringe pump, located at one end of the tube, in withdraw mode and simultaneously vertically moving the traverse/dipping stage into a reservoir containing both immiscible fluids. The traverse system and syringe are controlled and synced using a G-Code in order to generate droplet trains containing different dispersed phase lengths (L_D), carrier phase lengths (L_C). Carrier and dispersed phase lengths were varied by controlling the dwell speed of the dipper and the flow rate on the syringe pump. 10ml Hamilton glass syringes were used during testing to minimize any uncertainty due to deformation of the barrel and piston during the experiments.

The use of transparent tubing allowed droplet length, speed and spacing to be determined by means of two photodiodes and LEDs located along the tube, 1m apart from each other, as shown in Fig. 1. Photodiodes with integrated amplifiers (OPT301M), provided by Burr-Brown and white LEDs (as light sources) with a maximum voltage of 3.4 and current of $50mA$ were used in this experiment. As shown in Fig. 2(a), a plastic holder was designed to hold the sensor and the light source and maintain them orthogonal to the tube axis. As a droplet passes each photodiode, the light intensity from white-LEDs to the photodiode changes due to reflection and different refractive indices of the carrier and dispersed liquids. This change in light intensity results in a change in the voltage output of the photodiode and is recorded as a step change (see Fig.

2(b)). The data was recorded at $1kHz$ and analyzed using MATLAB to determine slug length (L_C), droplet length (L_D) and velocity of each droplet (U_D).

The results from length measurements show an excellent consistency in droplet length with the maximum variation of 6%.

Pressure drop was recorded using a Honeywell gauge pressure transducer (26PCCFA6D) with ±1, ±5 and ±15 PSI

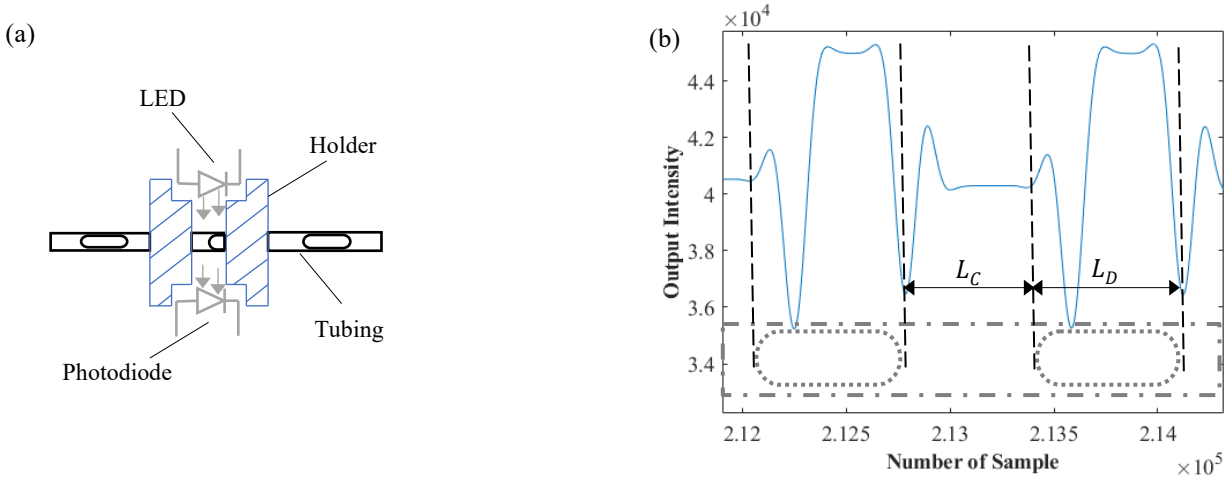

Fig. 2: (a) Light sensor configuration and (b) example of recorded data used for droplet velocity and length measurements.

range, 1ms response time, 6.67 mV/psi sensitivity and linearity of 0.5%. The pressure sensor is located within 0.5 m from the syringe pump and connected to the FEP tube with a T-Junction connector. Prior to use, the transducer was calibrated using laminar flow theory for a single phase fluid in a circular tube.

Silicon oil AR20, fluorinert™ FC40, hydrofluoroether HFE7500 and deionized water (DI water) were used in this study as the working liquids. Prior to experimentation, all liquids were filtered (using Millex® sterile syringe filter with a 0.45µm pore size) twice to remove any trace impurities. Afterwards, the surface and interfacial tension of all liquids were measured using a commercial CAM 2000 Pendant Drop system. A CCD camera with maximum frame rate of 30 fps was used for visualization purposes. Thermophysical properties of the fluids and range of dimensionless groups investigated in this are tabulated in Table.1 and 2 respectively.

Table 1: Thermophysical properties of the fluids investigated at **23**℃.

Liquid	Density (kg/m^3)	Viscosity (kg/ms)
Water	998	0.0009
FC40	1854	0.0039
HFE7500	1620	0.00124
AR20	1142	0.0209

Table 2: Range of dimensionless groups investigated in current study.

Carrier/Dispersed	Interfacial Tension(γ) (N/m)	Re_C	Ca_C	L_C^*	L_D^*	We	Viscosity Ratio ($\mu^* = \mu_C/\mu_D$)
AR20/Water	0.03	1.7×10^{-1} 9.4×10^{-1}	4×10^{-3} 2.2×10^{-2}	5.6-7.6	3.6-15.2	7.1×10^{-4} 2.3×10^{-2}	23.2
FC40/Water	0.051	2.9 14.8	9.6×10^{-4} 5×10^{-3}	4.9-7.8	4.1-15.3	2.7×10^{-3} 6.8×10^{-2}	4.33
HFE7500/Water	0.049	8.5 45	2.9×10^{-4} 1.5×10^{-3}	6-7.6	6.2-13.7	2.5×10^{-3} 6.2×10^{-2}	1.37
FC40/AR20	0.0061	2.6 13.8	9.2×10^{-3} 5.1×10^{-2}	3.2-7.2	3.3-12.4	2.3×10^{-2} 5.7×10^{-1}	0.18
HFE7500/AR20	0.0019	8.6 44	8×10^{-3} 4.5×10^{-2}	3.8-6.3	4-7.3	6×10^{-2} 1.6	0.059

4. Results and Discussion

This section presents a comprehensive comparison between experimental pressure drop results and the most well-known models for liquid-liquid Taylor flows proposed by Jovanović *et al*.,[9] and Mac Giolla Eain *et al*.,[10]. First results will be compared with both models by Jovanović *et al*.,[9] (Eq 2 and 3), and in the following by the model from Mac Giolla Eain *et al*.,[10] (Eq. 4).

4. 1. Moving and Stagnant Film Models

In Fig. 3 experimental results are compared with the moving-film model described in Eq. 3. In this graph, Y-axis and X-axis indicate experimental and the theoretical values of pressure drop respectively and $\pm 20\%$ deviations from the model are presented by dashed lines to evaluate accuracy of the model. From Fig. 3, it is evident that the model underpredicts the results in all cases. Results from experiments with HFE7500-water and FC40-water have been significantly underestimated by the model, while the results from AR20-water, HFE7500-AR20 and FC40-AR20 show a better agreement.

The current study shows an averaged deviation of 292% and 389% from the model for FC40-water and HFE7500-water examinations respectively. In AR20-water, FC40-AR20 and HFE7500-AR20 cases, although the model presents a better agreement with the averaged deviations of 20%, 12% and 14%, but still the results are underestimated by the correlation. Underestimating the pressure drop by this model has been shown also by Mac Giolla Eain *et al*.,[11] and can be explained by the procedures taken to achieve the model. As stated in the theory section, this model employs the theoretical solution of Bretherton to estimate the pressure drop caused by interfacial tension between phases. Taking this approach to determine the interfacial contribution in pressure drop resulted in neglecting the inertial effects and assuming a negligible liquid film thickness to radius ratio ($\frac{h}{R} < 0.01$)[9]. While several studies show that these assumption are valid for low Reynolds ($Re < 1$) number within a certain Capillary number range ($10^{-4} < Ca < 10^{-1}$)[13]. The effect of flow velocity on film thickness value and droplet morphology are presented in Fig.4. In Fig. 4(a), film thickness magnitudes have been determined by employing the model developed by Mac Giolla Eain *et al*.,[14] for liquid-liquid slug flow regimes. As expected, film thickness increases with velocity and for liquid-liquid combinations, with high Capillary numbers and a large viscosity difference (see Table. 2), the magnitude of the film thickness is significantly greater than cases with a relatively low Capillary number and $\mu^* \approx 1$ (such as HFE7500-water). Therefore, assuming negligible film thickness can be valid only for flows with a very low velocity and by increasing the flow velocity, the assumption becomes more inacceptable. As a matter of fact, mismatching the experimental and theoretical values in Fig. 3 can be justified by inability of the model to provide an appropriate prediction of the interfacial contribution in the overall pressure drop. In cases with carrier to droplet viscosity ratios greater than unity (AR20-water, FC40-water and HFE7500-water), results from AR20-water tests with the relatively lowest Reynold number range and the lowest value of the interfacial tension show a better agreement with the correlation. In both models proposed by Jovanović *et al*.,[9], the carrier phase and interfaces play the main roles in total pressure drop

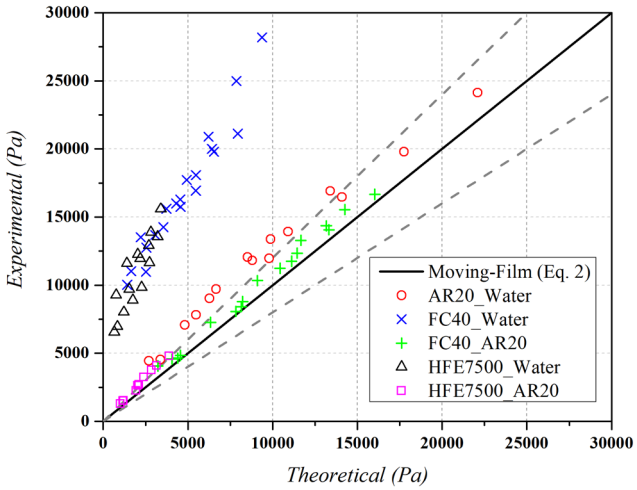

Fig. 3: Experimental pressure drop results plotted versus theoretical prediction calculated using moving-film model described by Eq. 2.

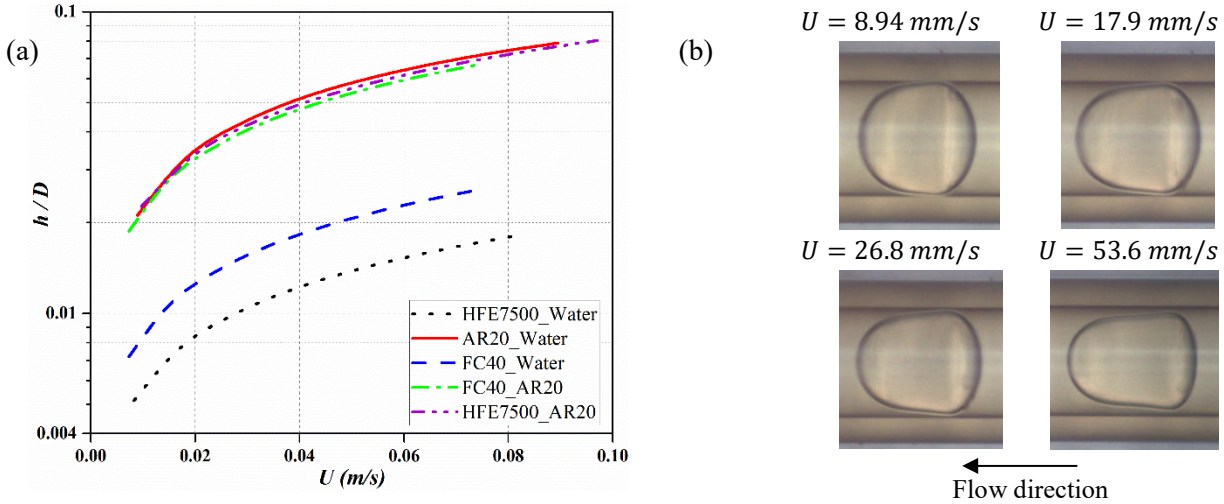

Fig. 4: (a) Effect of flow velocity on film thickness values and (b) images of water dispersed in AR20 over varying velocity but constant droplet volume.

value (88% to 94%) for the tested flows with $\mu^* > 1$; thus, decreased interfacial pressure drop contribution (by decreasing the interfacial tension value) and increased contribution of the carrier phase in the pressure drop (by increasing viscosity ratio) resulted in better agreement of experimental data with the model.

In experiments with $\mu^* < 1$, the model represents a good prediction of pressure drop for both flow combinations of FC40-AR20 and HFE7500-AR20 with the averaged deviations of 12% and 14% respectively. As discussed formerly, the main reason refers to the reduced interfacial tension involvement on total pressure drop. FC40-AR20 and HFE7500-AR20 with interfacial tension of 0.0061 and 0.0019 have the minimum values of the interfacial tension among the tested flows in this study. As a matter of fact the contribution of the interfacial pressure drop becomes very small, 4%-7%, and dispersed phase due to the high viscosity has a greater influence on the overall pressure drop. Hence, as the contribution of interfacial pressure to the total pressure is reduced the moving-film model is better positioned to predict the pressure drop for FC40-AR20 and HFE7500-AR20 flows.

In Fig. 5 results have been compared with the stagnant-film model (Eq.3). For flows with viscosity ratio greater than one, both moving and stagnant models present a very similar prediction. This similarity has been pointed out by the authors

with the relative difference of less than 1.4% in pressure drop prediction. While unlike the moving-film model that shows a good agreement for flows with the viscosity ratios less than one, the stagnant-film model overestimates the results by averaged deviation values of 65% and 94% for FC40-AR20 and HFE7500-AR20 experiments respectively. Looking at the model's equation(Eq.3), only the dispersed phase's viscosity has been incorporated in the term that defines the contribution of the dispersed phase in total pressure drop. While in the moving-film model, viscosities of both phases have been taken into account. Thus, this overpredicting is not surprising by considering the fact that AR20 with a high viscosity has been employed in both flows as the dispersed phase. In flows with low interfacial tension values, the impact of interfacial pressure on total pressure drop becomes weak and the remaining terms (the dispersed and carrier phase viscous pressure drop) dominate. Therefore, even a small miscalculation of the contribution of either dispersed phase or carrier phase can have a great effect on the overall predicted value of total pressure drop. On the other hand, thicker liquid film that surrounds the droplets of AR20 in FC40-AR20 and HFE7500-AR20 undermines validity of the stagnant-film assumption. For example, calculated film thickness ratio ($\frac{h}{D}$) from experiments by HFE7500-AR20, presents values almost three times greater than HFE7500-water (see Fig. 4(b)). The stagnant-film model was developed by assuming immobile flow within the film that encapsulates the droplet. However, this simplified assumption to approach the problem may not lead to a reliable solution in all cases. Figure. 5(b) illustrates a schematic of the velocity profile along the cross-section of the capillary and velocity

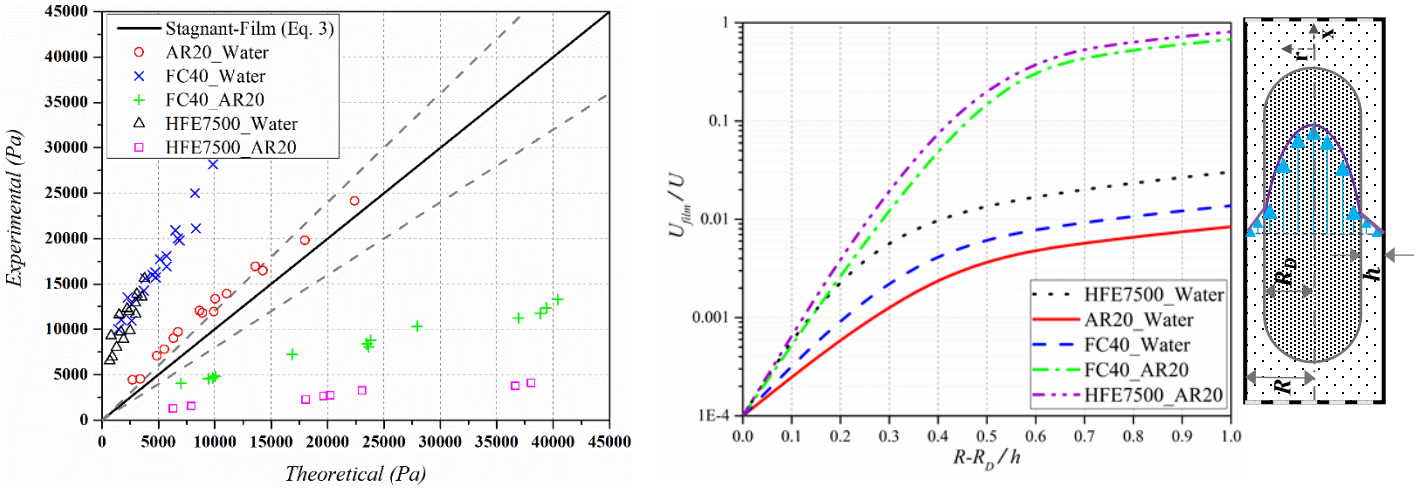

Fig. 5: (a) Experimental pressure drop plotted against theoretical prediction calculated using stagnant-film model described by Eq. 3. (b) Schematic of the velocity profile over the capillary cross section and comparison of the relative velocity across the film for tested liquid-liquid flow combinations.

magnitudes across the liquid film for all the tested flow combinations. The velocity profiles across the film are plotted using an expression given by Howard and Walsh[15].In this graph, HFE7500-AR20 and FC40-AR20 flows with the viscosity ratios of 0.18 and 0.059 respectively, show a non-negligible flow within the film. In addition, these flow combinations develop a relatively thicker film thickness due to the very low viscosity ratios (see Fig. 4(a)); hence, a thicker film thickness and a higher velocity of the flow within the film undermine validity of the stagnant-film model in these cases.

4. 2. Skin Friction Model

Fig. 6 gives a comparison between experimental data and the skin-friction model (Eq. 4). Data from experiments with FC40-water and HFE7500-water, exhibit an excellent agreement with the model. While, the theoretical solution greatly overestimates the pressure drop magnitude for experiments with AR20-water, FC40-AR20 and HFE7500-AR20. Based on this modeling method, contribution of the interfaces in total pressure drop was determined by neglecting film thickness encompassing the droplet within the tube. This assumption has been shown to be incorrect by several studies. In current study, the model shows good agreement in experiments with FC40-water and HFE7500-water, which have the minimum film thickness among all the examined fluid combinations (see fig. 4(a)). While, the model greatly overestimates the results

from AR20-water, FC40-AR20 and HFE7500-AR20 with a relatively thicker film (almost four times thicker). The results show an averaged deviation of 48%, 64% and 84% from the model for AR20-water, FC40-AR20 and HFE7500-AR20 respectively. In experiments with FC40-AR20 and HFE7500-AR20, the contribution of the dispersed phase to the overall pressure drop becomes more significant due to a higher droplet viscosity and a reduced contribution of interfacial pressure drop caused by lower interfacial tension (see Table. 2). Therefore, assuming negligible film thickness resulted in greater divergence from the model in these cases.

Overall, conducting experiments over wide-ranged flow conditions allowed a thorough analysis of the existing models. Data analysis revealed that inaccurate estimation of pressure drop is attributed to the procedures and assumptions taken to develop the models. Finally, this study contributes to a better understanding of pressure drop measurements in liquid-liquid Taylor flows by addressing the strengths and weaknesses of previous models.

5. Conclusion

Pressure drop in liquid-liquid Taylor flow regimes was investigated experimentally by means of five different liquid-liquid combinations. A novel experimental set up was employed to ensure high accuracy and repeatability of the measurements. Results were compared with the most acceptable models in the literature and the accuracy of each model was shown to be limited to a certain test conditions. Data analysis revealed that inaccurate estimation of pressure drop is attributed to the procedures and assumptions taken to develop the models.

Comparing the experimental data with moving-film model proposed by Jovanović et al.,[9], showed that pressure drop was underestimated for all liquid combinations. While, in cases with a very low viscosity ratio and interfacial tension, the stagnant-film model overestimates the results. The inability of both models to correctly estimate pressure drop is mainly due to the employing the theoretical solution of Bretherton[12] in evaluating the interfacial pressure drop. Taking this approach

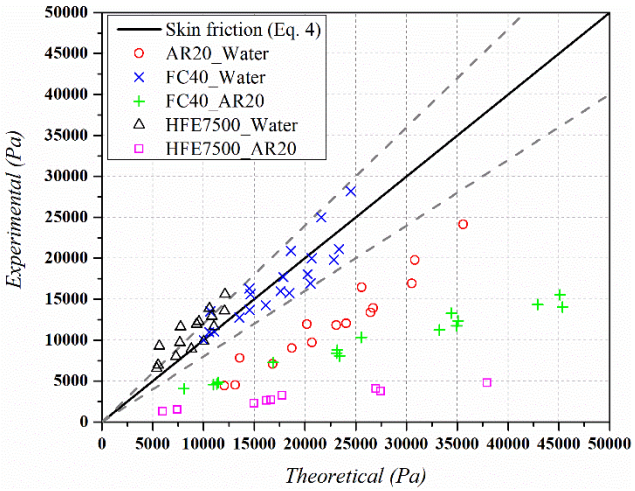

Fig. 6: Experimental pressure drop plotted against theoretical prediction calculated using skin-friction model described by Eq. 4.

results in assuming negligible inertial effects and liquid film thickness; while this approach is shown to be invalid in liquid-liquid flows due to the relatively higher inertial forces and formation of a thicker film surrounds the dispersed phase.

A comparison with the model proposed by Mac Giolla Eain et al.,[10] provided a better prediction of pressure drop in some cases but was still unable to make a correct estimation over the flows with a relatively thicker film around the droplet.

Overall, findings of the current study revealed that viscosity ratio of the involved phases can significantly affect the pressure drop in liquid-liquid flows, while no viscosity ratio-affected models have been proposed so far. As a result, a model that incorporates the effect of viscosity ratio is necessary to better estimate the pressure drop of liquid-liquid flows.

Finally, this study hopes to provide a foundation to establish a comprehensive model for accurately estimating pressure drop in liquid-liquid Taylor flow regimes in microchannels.

Acknowledgements

This research was supported by Science Foundation Ireland (SFI) [Grant Number: 13/RC/2007] through the SFI Research Centres Programme CONNECT.

References

[1] A. Abdollahi, S. E. Norris, and R. N. Sharma, "Fluid flow and heat transfer of liquid-liquid Taylor flow in square microchannels," *Applied Thermal Engineering,* vol. 172, p. 115123, 2020.

[2] M. M. G. Eain, V. Egan, and J. Punch, "Local Nusselt number enhancements in liquid–liquid Taylor flows," *International Journal of Heat and Mass Transfer,* vol. 80, pp. 85-97, 2015.

[3] H. F. Hamann, J. A. Lacey, Z. Hu, P. Bose, E. Cohen, J. Wakil, "Hotspot-limited microprocessors: Direct temperature and power distribution measurements," *IEEE Journal of Solid-State Circuits,* vol. 42, no. 1, pp. 56-65, 2006.

[4] S. K. Roy and B. L. Avanic, "A very high heat flux microchannel heat exchanger for cooling of semiconductor laser diode arrays," *IEEE Transactions on Components, Packaging, and Manufacturing Technology: Part B,* vol. 19, no. 2, pp. 444-451, 1996.

[5] M. Fabbri, S. Jiang, and V. K. Dhir, "A comparative study of cooling of high power density electronics using sprays and microjets," *J. Heat Transfer,* vol. 127, no. 1, pp. 38-48, 2005.

[6] T. Hotta and N. Patil, "A review on cooling of discrete heated modules using liquid jet impingement," *Frontiers in Heat and Mass Transfer (FHMT),* vol. 11, 2018.

[7] N. M. Jeffers, J. Punch, E. J. Walsh, and M. McLean, "Heat transfer from novel target surface structures to a normally impinging, submerged and confined water jet," *Journal of Thermal Science and Engineering Applications,* vol. 1, no. 3, 2009.

[8] M. Ebadian and C. Lin, "A review of high-heat-flux heat removal technologies," *Journal of heat transfer,* vol. 133, no. 11, 2011.

[9] J. Jovanović, W. Zhou, E. V. Rebrov, T. Nijhuis, V. Hessel, and J. C. Schouten, "Liquid–liquid slug flow: hydrodynamics and pressure drop," *Chemical Engineering Science,* vol. 66, no. 1, pp. 42-54, 2011.

[10] M. Mac Giolla Eain, V. Egan, J. Punch, P. Walsh, and E. Walsh, "An Investigation of the Pressure Drop Associated With Liquid-Liquid Slug Flows," in *International Conference on Nanochannels, Microchannels, and Minichannels*, 2013, vol. 55591: American Society of Mechanical Engineers, p. V001T03A009.

[11] M. M. G. Eain, V. Egan, J. Howard, P. Walsh, E. Walsh, and J. Punch, "Review and extension of pressure drop models applied to Taylor flow regimes," *International Journal of Multiphase Flow,* vol. 68, pp. 1-9, 2015.

[12] F. P. Bretherton, "The motion of long bubbles in tubes," *Journal of Fluid Mechanics,* vol. 10, no. 2, pp. 166-188, 1961.

[13] P. Aussillous and D. Quéré, "Quick deposition of a fluid on the wall of a tube," *Physics of fluids,* vol. 12, no. 10, pp. 2367-2371, 2000.

[14] M. M. G. Eain, V. Egan, and J. Punch, "Film thickness measurements in liquid–liquid slug flow regimes," *International Journal of heat and fluid flow,* vol. 44, pp. 515-523, 2013.

[15] J. A. Howard and P. A. Walsh, "Review and extensions to film thickness and relative bubble drift velocity prediction methods in laminar Taylor or slug flows," *International journal of multiphase flow,* vol. 55, pp. 32-42, 2013.